De novo biosynthesis of diverse plant-derived styrylpyrones in *Saccharomyces cerevisiae*

Yinan Wu [a], Maple N. Chen [b], Sijin Li [a],*

[a] *Robert F. Smith School of Chemical and Biomolecular Engineering, Cornell University, Ithaca, NY, 14853, USA*
[b] *Nancy E. and Peter C. Meinig School of Biomedical Engineering, Cornell University, Ithaca, NY, 14853, USA*

ABSTRACT

Plant styrylpyrones exerting well-established neuroprotective properties have attracted increasing attention in recent years. The ability to synthesize each individual styrylpyrone in engineered microorganisms is important to understanding the biological activity of medicinal plants and the complex mixtures they produce. Microbial biomanufacturing of diverse plant-derived styrylpyrones also provides a sustainable and efficient approach for the production of valuable plant styrylpyrones as daily supplements or potential drugs complementary to the prevalent agriculture-based approach. In this study, we firstly demonstrated the heterogenous biosynthesis of two 7,8-saturated styrylpyrones (7,8-dihydro-5,6-dehydrokavain (DDK) and 7,8-dihydroyangonin (DHY)) and two 7,8-unsaturated styrylpyrones (desmethoxyyangonin (DMY) and yangonin (Y)), in *Saccharomyces cerevisiae*. Although plant styrylpyrone biosynthetic pathways have not been fully elucidated, we functionally reconstructed the recently discovered kava styrylpyrone biosynthetic pathway that has high substrate promiscuity in yeast, and combined it with upstream hydroxycinnamic acid biosynthetic pathways to produce diverse plant-derived styrylpyrones without the native plant enzymes. We optimized the *de novo* pathways by engineering yeast endogenous aromatic amino acid metabolism and endogenous double bond reductases and by CRISPR-mediated *δ*-integration to overexpress the rate-limiting pathway genes. These combinatorial engineering efforts led to the first three yeast strains that can produce diverse plant-derived styrylpyrones *de novo*, with the titers of DDK, DMY and Y at 4.40 μM, 1.28 μM and 0.10 μM, respectively. This work has laid the foundation for larger-scale styrylpyrone biomanufacturing and the complete biosynthesis of more complicated plant styrylpyrones.

1. Introduction

Styrylpyrones are an important group of phenylpropanoid natural products found in fungi and plants (Table 1) (Lee and Yun, 2011; Zhang et al., 2018). Fungal styrylpyrones are usually found in mushrooms belonging to the Hymenochaetaceae family. Considered as the fungal counterparts of bioactive in plants, fungal styrylpyrones are postulated to be the natural products leading to the pharmaceutical bioactivity of medicinal mushrooms in traditional medicine (Lee and Yun, 2011). A number of fungal styrylpyrones have been isolated and identified, including hispidin, bisnoryangonin, and their derivatives; yet their biosynthetic pathways or potential pharmaceutical effects have not been systematically investigated. Meanwhile, plant styrylpyrones exhibit higher chemical diversity and structural complexity, along with relatively well-identified pharmacological properties *in vivo*, *in vitro*, and in animal models (Bian et al., 2020; Sarris et al., 2013; Smith and Leiras,

2018; Tu and Tawata, 2014). Plant styrylpyrones are mostly reported in angiosperm plants, including Piperaceae, Lauraceae, Annonaceae, Ranuculaceae and Zingiberaceae, and play an important role in plant defense against attacks (Beckert et al., 1997). In particular, a group of plant styrylpyrones with the unique C-4 methyl group on the pyrone ring, namely kavapyrones (or kavalactones), have exhibited significant anxiolytic, analgesic, or neuroprotective effects (Tzeng and Lee, 2015). Kavalactones derived from a representative plant producer kava (*Piper methysticum*) have been proven to be the active ingredients leading to the psychoactive effect of the kava extracts and kava beverages that are becoming increasingly popular globally, examples including yangonin (Y), desmethoxyyagonin (DMY), kavain (K), dihydrokavain (DHK), methysticin (M) and dihydromethysticin (DHM). Styrylpyrones found in other plants that are non-psychoactive also exhibit great potential: for example, 7,8-dihydro-5,6-dehydrokavain (DDK) is the major bioactive component found in shell ginger (*Alpinia zerumbet*) (35% of the total
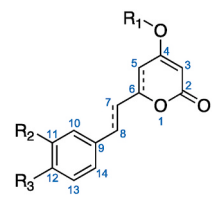
Table 1
Names and structures of representative styrylpyrones.

	R_1	R_2	R_3	C5-C6	C7-C8
Fungal styrylpyrone					
Hispidin	H	OH	OH	=	=
Bisnoryangonin	H	H	OH	=	=
Plant-derived styrylpyrone					
Desmethoxyyagonin (DMY)	CH_3	H	H	=	=
Kavain (K)	CH_3	H	H	–	=
Dihydrokavain (DHK)	CH_3	H	H	–	–
Yangonin (Y)	CH_3	H	OCH_3	=	=
Methysticin (M)	CH_3	OCH_2O		–	=
Dihydromethysticin (DHM)	CH_3	OCH_2O		–	–
7,8-Dihydro-5,6-dehydrokavain (DDK)	CH_3	H	H	=	–
7,8-Dihydroyangonin (DHY)	CH_3	H	OCH_3	=	–

fresh rhizome weight), a cuisine and medicinal plant in East Asia with nutritional and pharmaceutical uses in traditional medicine (Teschke and Xuan, 2018; Xuan and Teschke, 2015).

As important herbal supplements, plant styrylpyrones are consumed in the form of plant extracts (e.g., kava extract for the functional beverage industry), which relies solely on time-consuming agricultural processes. These traditional approaches cannot meet the growing global demand of valuable plant styrylpyrones, especially the increasing demand of anxiolytic kavalactones. Harvesting and extracting styrylpyrones from their native plant producers is susceptible to climate changes; while the unstable and inconsistent supply from various cultivars, along with the laborious and time-consuming cultivation process (three to five years for kava and 10–12 months for *A. zerumbet*) further increases the cost. Additionally, the complexity of plant extracts hinders efficient styrylpyrone isolation and production, which hinders the investigation of their pharmacological effects. While chemical synthesis is an alternative solution for the production of plant natural products (PNPs), only a few kavalactones and their derivatives have been chemically synthesized at laboratory scales with yields ranging from 30% to 60% (Ali Shaik et al., 2012; Israili and Smissman, 1976; Kraus and Wanninayake, 2015; Lin et al., 2008; Volgin et al., 2020). The poor stereospecificity and the involvement of heave metals as catalysts further hinders large-scale chemical synthesis.

Microbial biomanufacturing of PNPs provides a new strategy to address the challenges associated with agricultural or chemical approaches. Advances in next-generation sequencing and bioinformatics have accelerated the identification of PNP biosynthetic pathway genes by comparative plant genomics or transcriptomics analyses; the development of synthetic biology and metabolic engineering methods has enabled high-throughput, heterologous plant pathway reconstruction and characterization (Han et al., 2021; S. Li et al., 2018; Pyne et al., 2019). Hundreds of PNP biosynthetic pathways have been reconstructed and engineered in industrial microbial hosts such as *Escherichia coli* or *Saccharomyces cerevisiae*, leading to the pilot or industrial-scale biomanufacturing of multiple PNPs (Courdavault et al., 2021; Song et al., 2014). In particular, *S. cerevisiae*, or baker's yeast, is of unique importance for the industrial biomanufacturing of PNPs with complex structures, due to the fast growth rate, abundance of engineering and fermentation tools, and higher similarity with plant cells that provides similar subcellular compartments for plant enzymes compared to bacterial hosts.

The formation of the styrylpyrone scaffold in plant is catalyzed by styrylpyrone synthase (SPS), a polyketide synthase (PKS) that condenses one hydroxycinnamoyl-CoA with two malonyl-CoA molecules. The biochemical function of plant SPS has been firstly characterized using cell free extracts from the common horsetail *Equisetum arvense* in late 1990s (Beckert et al., 1997); yet the genes in the biosynthetic pathway leading to plant styrylpyrones remained unexplored until recently. By exploiting *de novo* transcriptome assembly, phylogenomics, and expression analysis, a recent work has identified the genes encoding SPS and downstream tailoring enzymes (methyltransferases catalyzing methylation at multiple sites, including the C4 site that distinguishes plant and fungal styrylpyrones, and oxidoreductases catalyzing the reduction of the 5,6-olefin and the formation of the C11-C12 methylenedioxy bridge) from the kava plant for the first time (Pluskal et al., 2019). An SPS-like enzyme, PnPKS, has also been reported from the black pepper (*Piper nigrum*) transcriptome, catalyzing feruloyl-CoA into 11-methoxy-bisnoryangonin (Heo et al., 2021). Although the discovery of the core styrylpyrone pathway genes in plants has laid the foundation for the engineered biosynthesis of plant styrylpyrones heterologously, microbial production of plant-specific styrylpyrone has not been achieved: while yangonin and methysticin can be synthesized in the model plant *Nicotiana benthamiana* via transient gene co-expression (Pluskal et al., 2019), microbial production of plant-specific styrylpyrones has never been reported.

In this study, we reconstituted the plant styrylpyrone pathway in yeast to produce four plant-derived styrylpyrones from hydroxycinnamic acid precursors. Products include three kavalactones (DMY, Y, and DHY) and one *A. zerumbet*-derived styrylpyrone (DDK). We then engineered the yeast endogenous metabolism and rebuilt upstream hydroxycinnamic acid pathway for the complete synthesis of DDK (0.69 μM), DMY (0.053 μM) and Y (0.0056 μM), respectively. By further overexpressing the bottleneck enzymes using high-copy plasmids and then CRISPR-mediated genomic δ-integration, the production was further enhanced (DDK, DMY and Y at 4.40 μM, 1.28 μM and 0.10 μM, respectively). We anticipate that these yeast strains will enable more complicated plant styrylpyrone biosynthesis and modification, and pave the way towards larger-scale valuable plant styrylpyrone biomanufacturing.

2. Material and methods

2.1. Chemicals, enzymes, kits and oligonucleotides

Yeast nitrogen base (YNB) and amino acid mixtures were purchased from Sunrise Science Products. Ammonium sulfate, dithiothreitol (DTT), *p*-coumaric acid and *p*-hydrocoumaric acid were purchased from Sigma-Aldrich. DDK was purchased from Toronto Research Chemicals. DMY and Y were purchased from Neta. 5-Fluoroorotic acid was purchased from Zymo Research. All other chemicals, including antibiotics, were purchased from VWR International or Fisher Scientific.

Q5 High-Fidelity 2X Master Mix, OneTaq Quick-Load 2X Master Mix, Gibson Assembly Master Mix, T4 polynucleotide kinase, Golden Gate Assembly Kit, EcoRI-HF restriction enzyme, DNA ladder and gel loading dye were purchased from New England Biolabs. Gateway LR Clonase II Enzyme mix was purchased from Life Technologies. Lyticase from *Arthrobacter luteus* was purchased from Sigma-Aldrich. Plasmid miniprep, gel DNA recovery, yeast genomic DNA Kit, *E. coli* transformation and frozen-EZ yeast transformation II kits were purchased from Zymo Research.

DNA sequences were synthesized by Twist Bioscience. Oligonucleotide primers (listed in Supplementary Table S2) were synthesized by Life Technologies.

2.2. Strains, plasmids, media and culture conditions

The host strains and plasmids used in this study are summarized in Table 2. Comprehensive information about their constructions is described in the following. Overall, all engineered yeast strains were

Table 2
List of strains and plasmids used in this study.

	Description	Genotype	Reference
Strains			
Top10	*E. coli* Top10		ATCC
CEN.PK2-1D	yeast CEN.PK2-1D	*MATα, URA3-52, TRP1-289, LEU2-3112, HIS3Δ1, MAL2-8C, SUC2*	EUROSCARF
ySL80	*TSC13* replaced CEN.PK2-1D	CEN.PK2-1D, *ΔTSC13::MdECR*	This study
ySL81	CEN.PK2-1D integrated with downstream kavalactone pathway	CEN.PK2-1D, *ΔYDR514C*::T_{PH5O}-*yPmKOMT1*-P_{PGK1}-*HIS5*-T_{STE2}-*yAt4CL3*-P_{TPI1}-P_{TEF1}-*yPmSPS1*-T_{CYC1}	This study
ySL82	ySL80 integrated with downstream kavalactone pathway	ySL80, *ΔYDR514C*::T_{PH5O}-*yPmKOMT1*-P_{PGK1}-*HIS5*-T_{STE2}-*yAt4CL3*-P_{TPI1}-P_{TEF1}-*yPmSPS1*-T_{CYC1}	This study
ySL83	Normal cinnamic acid overproducer	CEN.PK2-1D, *ΔYBL059W*::*ARO4*^{Q166K}-*ARO7*^{T226I}-*HygR*-P_{GPD1}-*TKL1*-T_{ADH1}-T_{PH5O}-*yAtPAL1*-P_{PGK1}	This study
ySL84	Cinnamic acid overproducer with *TSC13* replaced	ySL80, *ΔYBL059W*::*ARO4*^{Q166K}-*ARO7*^{T226I}-*HygR*-P_{GPD1}-*TKL1*-T_{ADH1}-T_{PH5O}-*yAtPAL1*-P_{PGK1}	This study
ySL85	Normal *p*-coumaric acid overproducer	CEN.PK2-1D, *ΔYBL059W*:*ARO4*^{Q166K}-*ARO7*^{T226I}-*HygR*-P_{GPD1}-*TKL1*-T_{ADH1}-T_{PH5O}-*yRsTAL1*-P_{PGK1}	This study
ySL86	*p*-Coumaric acid overproducer with *TSC13* replaced	ySL80, *ΔYBL059W*::*ARO4*^{Q166K}-*ARO7*^{T226I}-*HygR*-P_{GPD1}-*TKL1*-T_{ADH1}-T_{PH5O}-*yRsTAL1*-P_{PGK1}	This study
ySL87	*De novo* DDK producer	ySL83, *ΔYDR514C*::T_{PH5O}-*yPmKOMT1*-P_{PGK1}-*HIS5*-T_{STE2}-*yAt4CL3*-P_{TPI1}-P_{TEF1}-*yPmSPS1*-T_{CYC1}	This study
ySL88	*De novo* DMY producer	ySL84, *ΔYDR514C*::T_{PH5O}-*yPmKOMT1*-P_{PGK1}-*HIS5*-T_{STE2}-*yAt4CL3*-P_{TPI1}-P_{TEF1}-*yPmSPS1*-T_{CYC1}	This study
ySL89	*De novo* Y producer	ySL86, *ΔYDR514C*::T_{PH5O}-*yPmKOMT1*-P_{PGK1}-*HIS5*-T_{STE2}-*yAt4CL3*-P_{TPI1}-P_{TEF1}-*yPmSPS1*-T_{CYC1}	This study
ySL87-δ_SK	Selected DDK overproducer derived after δ-integration		This study
ySL88-δ_SK	Selected DMY overproducer derived after δ-integration		This study
ySL89-δ_SK	Selected Y overproducer derived after δ-integration		This study
Plasmids			
pSL2	Backbone template, pCS3688	*attL1*-P_{TPI1}-*ySl4CL1*-T_{STE2}-*attL2*	Smolke Lab
pSL3	Backbone template, pCS3689	*attL1*-P_{GPD1}-*ySlF3H*-T_{ADH1}-*attL2*	Smolke Lab
pSL4	Backbone template, pCS3690	*attL1*-P_{TEF1}-*ySlCYPR*-T_{CYC1}-*attL2*	Smolke Lab
pSL5	Backbone template, pCS3691	*attL1*-P_{PGK1}-*ySlCHS550*-T_{PH5O}-*attL2*	Smolke Lab
pSL56	*yPmSPS1* expression cassette	*attL1*-P_{TEF1}-*yPmSPS1*-T_{CYC1}-*attL2*	This study
pSL54	*yPmKOMT1* expression cassette	*attL1*-P_{PGK1}-*yPmKOMT1*-T_{PH5O}-*attL2*	This study
pSL85	*yAt4CL3* expression cassette	*attL1*-P_{TPI1}-*yAt4CL3*-T_{STE2}-*attL2*	This study
pSL26			Smolke Lab

Table 2 (*continued*)

	Description	Genotype	Reference
	ARO7^{T226I} expression cassette; *HIS5* maker, pCS3030	*attL1*-*ARO7*^{T226I}-*attL2*, *HIS5*	
pSL47	pCRCT template	pCRCT (pRS426-*iCas9*-*gRNA*, *URA3d*)	Shi et al., (2016)
pSL241	pCRCT for *TSC13* replacement	pRS426-*iCas9*-*TSC13_gRNA-1*, *URA3d*	This study
pSL242	pCRCT for *TSC13* replacement	pRS426-*iCas9*-*TSC13_gRNA-2*, *URA3d*	This study
pSL43	Backbone template	pRS424	ATCC
pSL45	Backbone template	pRS426	ATCC
pSL243	*yPmSPS1* overexpression (level: +)	pRS424-P_{TEF1}-*yPmSPS1*-T_{CYC1}, *TRP1*	This study
pSL244	*yPmKOMT1* overexpression (level: +)	pRS426-P_{PGK1}-*yPmKOMT1*-T_{PH5O}, *URA3*	This study
pSL245	*yAt4CL3* overexpression (level: +)	pRS424-P_{TPI1}-*yAt4CL3*-T_{STE2}, *TRP1*	This study
pSL246	*yAt4CL3* overexpression (level: +)	pRS426-P_{TPI1}-*yAt4CL3*-T_{STE2}, *URA3*	This study
pSL28	*ARO4*^{Q166K} expression cassette, pCS3028	*attL1*-*ARO4*^{Q166K}-*attL2*	Smolke Lab
pSL25	*HygR* marker template, pCS2922	*attL1*-*HygR*-*attL2*	Smolke Lab
pSL30	*TKL1* expression cassette	*attL1*-P_{GPD1}-*TKL1*-T_{ADH1}-*attL2*	This study
pSL118	*yAtPAL1* expression cassette, pCS4057	*attL1*-P_{PGK1}-*yAtPAL1*-T_{PH5O}-*attL2*	Smolke Lab
pSL11	*yRsTAL1* expression cassette, pCS4058	*attL1*-P_{PGK1}-*yRsTAL1*-T_{PH5O}-*attL2*	Smolke Lab
pSL86	*mCherry* expression cassette	*attL1*-P_{TEF1}-*mCherry*-T_{CYC1}-*attL2*	This study
pSL23	Backbone	pAG416-ccdB	ATCC
pSL247	*mCherry* overexpression	pAG416-P_{TEF1}-*mCherry*-T_{CYC1}, *URA3*	This study
pSL44	Backbone template	pRS425	ATCC
pSL202	Backbone	pRS425, *LEU2d*	This study
pSL203	Backbone	pRS426, *URA3d*	This study
pSL248	*mCherry* overexpression (level: +)	pRS425-P_{TEF1}-*mCherry*-T_{CYC1}, *LEU2*	This study
pSL249	*mCherry* overexpression (level: ++)	pRS425-P_{TEF1}-*mCherry*-T_{CYC1}, *LEU2d*	This study
pSL251	*mCherry* overexpression (level: +++)	pRS426-P_{TEF1}-*mCherry*-T_{CYC1}, *URA3d*	This study
pSL252	*yPmSPS1-yPmKOMT1* overexpression (level: +)	pRS425-T_{PH5O}-*yPmKOMT1*-P_{PGK1}-P_{TEF1}-*yPmSPS1*-T_{CYC1}, *LEU2*	This study
pSL253	*yPmSPS1-yPmKOMT1* overexpression (level: ++)	pRS425-T_{PH5O}-*yPmKOMT1*-P_{PGK1}-P_{TEF1}-*yPmSPS1*-T_{CYC1}, *LEU2d*	This study
pSL254	*yPmSPS1-yPmKOMT1* overexpression (level: +++)	pRS426-T_{PH5O}-*yPmKOMT1*-P_{PGK1}-P_{TEF1}-*yPmSPS1*-T_{CYC1}, *URA3d*	This study
pSL58	Backbone template	pTrc99A	Addgene
pSL255	Donor for δ integration of *mCherry*	pTrc99A-$δ_L$-P_{TEF1}-*mCherry*-T_{CYC1}-$δ_R$	This study
pSL27	*KLLEU2* marker template, pCS274	*attL1*-*KLLEU2*-*attL2*	Smolke Lab
pSL256	Donor for δ integration of *mCherry* with *KlLEU2d* marker	pTrc99A-$δ_L$-*KlLEU2d*-P_{TEF1}-*mCherry*-T_{CYC1}-$δ_R$	This study
pSL257	pCRCT for δ integration	pRS426-*iCas9*-*δ_gRNA*, *URA3d*	This study
pSL258	Donor for δ integration of *yPmKOMT1*[a]-*yPmSPS1*[a] with *KlLEU2d* marker	pTrc99A-$δ_L$-*KlLEU2d*-T_{PH5O}-*yPmKOMT1*[a]-P_{PGK1}-P_{TEF1}-*yPmSPS1*[a]-T_{CYC1}-$δ_R$	This study

[a] DNA sequence was optimized to remove EcoRI cutting sites.

constructed based on CEN.PK2-1D and cultured at 30 °C in synthetic complete (SC) or appropriate synthetic drop-out (SD) media (0.17% YNB, 0.5% ammonium sulfate, and 1 × amino acid complete or drop-out mixture) in 96-well deep-well plates, unless otherwise stated. Hygromycin was added to a final concentration of 200 μg/mL when appropriate; *E. coli* Top10 was used for gene cloning and plasmid extraction and were

cultured in LB medium containing appropriate antibiotics at 37 °C, 250 rpm in 14 mL plastic culture tubes. To make solid media plates, 2.5% agar was added additionally.

2.2.1. Plasmid construction

Plasmids were assembled by Gibson Assembly (Gibson et al., 2009) using Gibson Assembly Master Mix. DNA fragments were PCR amplified from template plasmids (Table 2), yeast genomic DNA, or synthesized DNA using the Q5 polymerase, and then purified by agarose gel extraction with a gel DNA recovery kit according to the manufacturer's instructions. Detailed information about their construction is listed in Supplementary Table S3. In addition, to allow for CRISPR/Cas9-mediated δ-integration, pSL241, pSL242 and pSL257 were developed based on the pCRCT plasmid (named as pSL47 in this study) (Bao et al., 2015) and constructed by Golden Gate Assembly. TSC13N201-PF/TSC13N201-PR, TSC13N202-PF/TSC13N202-PR and Delta-N20-PF/Delta-N20-PR primer pairs were annealed and phosphorylated to make the N20 inserts for pSL241, pSL242 and pSL257, respectively. To tune the overexpression level of pathways, low- and ultra-high-copy plasmids expressing the mCherry fluorescence protein (pSL247 and pSL251) were constructed using Gateway LR Clonase II Enzyme mix, pSL86 as the entry plasmids, pSL23 and pSL203 as the destination plasmids, respectively.

E. coli competent cells were made using an *E. coli* transformation kit according to the manufacturer's instructions. *E. coli* strains harboring plasmids were cultured in LB media with 50 μg/mL of kanamycin or 100 μg/mL of carbenicillin as appropriate. Plasmids were extracted using a plasmid miniprep kit according to the manufacturer's instructions, followed by concentration measurement through NanoDrop One (ThermoFisher Scientific) and Sanger Sequencing (GENEWIZ).

2.2.2. Yeast strain construction

2.2.2.1. Preparation of yeast electrocompetent cells.
Yeast genome integrations were performed by electroporation as demonstrated previously (Y. Li et al., 2018), a voltage of 540 V, capacitance of 25 μF and infinite resistance with a Gene Pulser Xcell Total System electroporator (Bio-Rad).

2.2.2.2. CRISPR/Cas9-mediated TSC13 replacement.
For CRISPR/Cas9-mediated genome editing, the pCRCT plasmid developed by Bao et al. (2015) was used and named as pSL47. To replace the native *TSC13* gene with a *Malus domestica* enoyl reductase gene (*MdECR*), the N20 region of pSL47 was changed to TACCTTGATTCAATGGGACA and TTCCATTACTGGGTTCTAAG using the CRISPR tool on Benchling (www.benchling.com), to yield pSL241 and pSL242, respectively. *MdECR* inserts were PCR amplified from synthesized gene fragments using the primers MdECR-PF/MdECR-PR, resulting in *MdECR* inserts with 35-bp overlaps to both the *TSC13* promoter and *TSC13* terminator on the yeast genome. 200 ng of *MdECR* inserts and 200 ng of either pSL241 or pSL242 were mixed and transformed into yeast strain CEN.PK2-1D by electroporation. The transformed cells were selected in 5 mL of SD-Ura media and incubated in a culture tube at 30 °C, 400 rpm for 48 h. After incubation, 1 mL of culture was spread on an SD-Ura plate for single colony growth. Successful integrants were verified through colony PCR analysis. pSL241 or pSL242 were removed via counter-selection in 1 mL of YPD with 10 μL of 5-FOA (100 mg/mL in dimethylsulfoxide) at 30 °C, 400 rpm for 24 h. Resultant plasmid-free cultures were streaked on a YPD plate and named ySL80.

2.2.2.3. Pathway integration.
DNA inserts containing pathway genes, auxotrophic marker genes, and 500- or 1000-bp genomic homologies, each harboring 25-bp overlaps between adjacent fragments, were PCR amplified from plasmids or yeast genomic DNA (Supplementary Table S4) and transformed at equimolar ratios into yeast by electroporation. The transformed cells were immediately mixed with 1 mL of YPD medium and recovered at 30 °C, 400 rpm for 2 h, then harvested by centrifugation (8000 rpm, 1 min) and spread on selection plates for 2–3 days of growth. The correctly assembled constructs were verified through colony PCR analysis.

2.2.2.4. CRISPR/Cas9-mediated δ-integration by electroporation.
To enable multiplex δ-integration, the N20 on pSL47 was replaced with δ site-specific N20 TATACTAGAAGTTCTCCTCG (Shi et al., 2016), resulting in pSL257. Two donor plasmids containing mCherry expression cassettes and/or truncated auxotrophic marker cassettes were constructed, including pSL255 (containing δ_L-mCherry-δ_R) and pSL256 (containing δ_L-KlLEU2d-mCherry-δ_R). The inserts were obtained by digesting donor plasmids with EcoRI-HF enzymes, followed by agarose gel recovery. δ-integration was firstly tested by mixing pSL257 with gradient amounts of δ_L-mCherry-δ_R inserts for electroporation. Due to the high false-positive ratio, δ_L-KlLEU2d-mCherry-δ_R (pSL256) that contains both mCherry and an auxotrophic selection marker was developed and used in the following experiments: 500 ng of pSL257 was mixed with 2 μg of δ_L-KlLEU2d-mCherry-δ_R inserts and transferred into CEN.PK2-1D by electroporation. The transformed cells were immediately mixed with 1 mL of YPD medium and recovered at 30 °C, 400 rpm for 1 h. Yeast cells harvested by centrifugation at 10000 rpm for 1 min were then selected in SD-Ura-Leu liquid and plate media. The optimized method led to higher integration efficiency and was used for following pathway integrations.

For the δ-integration of pathways, codon-optimized genes encoding kava styrylpyrone synthase 1 (*yPmKOMT1*) and *O*-methyltransferases 1 (*yPmSPS1*) were inserted into pSL256 to replace *mCherry*, resulting in pSL258. 500 ng of pSL257 were mixed with the pathway inserts and transferred into ySL87, ySL88 and ySL89 by electroporation. Cells were selected on SD-Ura-Leu plates and then cultured in liquid SD-Ura-Leu media at 30 °C, 400 rpm for 3 days. The product titers in the cultures were measured, and populations with higher titers were streaked on SD-Ura-Leu plates. After 2–3 days of growth, several colonies were picked and incubated in SD-Leu media in culture tubes at 30 °C, 400 rpm for 24 h respectively. Product titers were measured and the cultures with higher titers were transferred into SD-Leu(5-FOA) media for 24 h of counter-selection to remove pSL257. Resultant plasmid-free cultures were streaked on SD-Leu plates for further screening.

2.2.3. Chemical transformation of plasmids into yeast host

Chemically competent yeast cells were prepared using frozen-EZ yeast transformation II kits according to the manufacturer's instructions. For single-plasmid transformation, 200 ng of plasmids were used while for double-plasmid transformation, 500 ng of each plasmid was used. After transformation, cells were spread on an appropriate selection plate and incubated at 30 °C for 2–3 days to allow for the growth of transformants.

2.3. Fermentation and sample preparation

Fresh yeast strains from plates were first incubated in 0.5 mL of SC, corresponding SD, or YP media supplemented with 2% dextrose in 96-well deep-well plates at 30 °C, 400 rpm in triplicates for 24 h and then transferred into 0.5 mL of corresponding fresh media for 48 h. For substrate (cinnamic acid, hydrocinnamic acid, *p*-coumaric acid and *p*-hydrocoumaric acid) feeding assays, 200 μM of substrates were tested as substrates for product production. 75 μL of each culture was harvested and mixed with 75 μL of methanol for sample preparation. Samples were filtered in 96-well filter plates (Pall Laboratory) and analyzed by HPLC/MS.

2.4. Metabolite analysis

Metabolites were identified and quantified by HPLC/Q-TOF (Agilent 1260 Infinity II/Agilent G6545B) in MS mode using positive ionization. For analysis, 1 μL of each culture sample was injected and separated in the ZORBAX RRHD Eclipse Plus C18 column (2.1 × 50 mm, 1.8 μm) (Agilent) with water with 0.1% formic acid (A) and acetonitrile with 0.1% formic acid (B) as the mobile phase. The gradient program was set as 0–1 min, 95% A; 1–11 min, 95%–5% A; 11–13 min, 5% A; 13–14 min, 5%–95% A; and 14–16 min, 95% A at a flow rate of 0.4 mL/min. The m/z value of the $[M+H]^+$ adduct was then used to extract the ion chromatogram (with a mass error below 20 ppm) for compound identification and quantification (see Supplementary Fig. S1 for extracted ion chromatograms of DDK, DMY, and Y standard). For compounds with available chemical standards, including cinnamic acid, hydrocinnamic acid, p-coumaric acid, p-hydrocoumaric acid, DDK, DMY, and Y, concentrations were quantified by comparing the integrated peak areas to standard curves (Supplementary Fig. S2 and Fig. S3). For identification of compounds of which no standards are available, target MS/MS mode with three different levels of collision energy (10, 20 and 40 eV) was used in addition to high-resolution MS analysis.

2.5. mCherry intensity measurement

To measure the gene overexpression level in plasmids or integrated yeasts, mCherry intensity in different yeasts and vectors was tested. 20 μL of overnight yeast cultures were transferred into 80 μL of Milli-Q water in clear-bottomed 96-well microplates for measurement of OD_{600} and mCherry fluorescence. Using a microplate reader (Infinite M1000 Pro, TECAN), mCherry fluorescence was measured using an excitation wavelength of 587 nm and emission wavelength of 610 nm and normalized by OD_{600}.

2.6. Robustness test of yeast overproducers after δ-integration

To test the robustness of yeast strains after δ-integration, strains were serially transferred in 1 mL YPD media in culture tubes at 30 °C, 400 rpm seven times, in duplicates. In each serial dilution, 10 μL previous cultures were transferred into fresh YPD media and grown until saturation; soon after the saturation (24 h), new cultures were transferred to fresh YPD media and streaked on YPD plates. Given the 1:100 dilution, the cells were estimated to duplicate at least 6.64 times until re-saturation, which was approximated as seven generations per day in this study (Blount et al., 2008). Finally, strains from different generations were
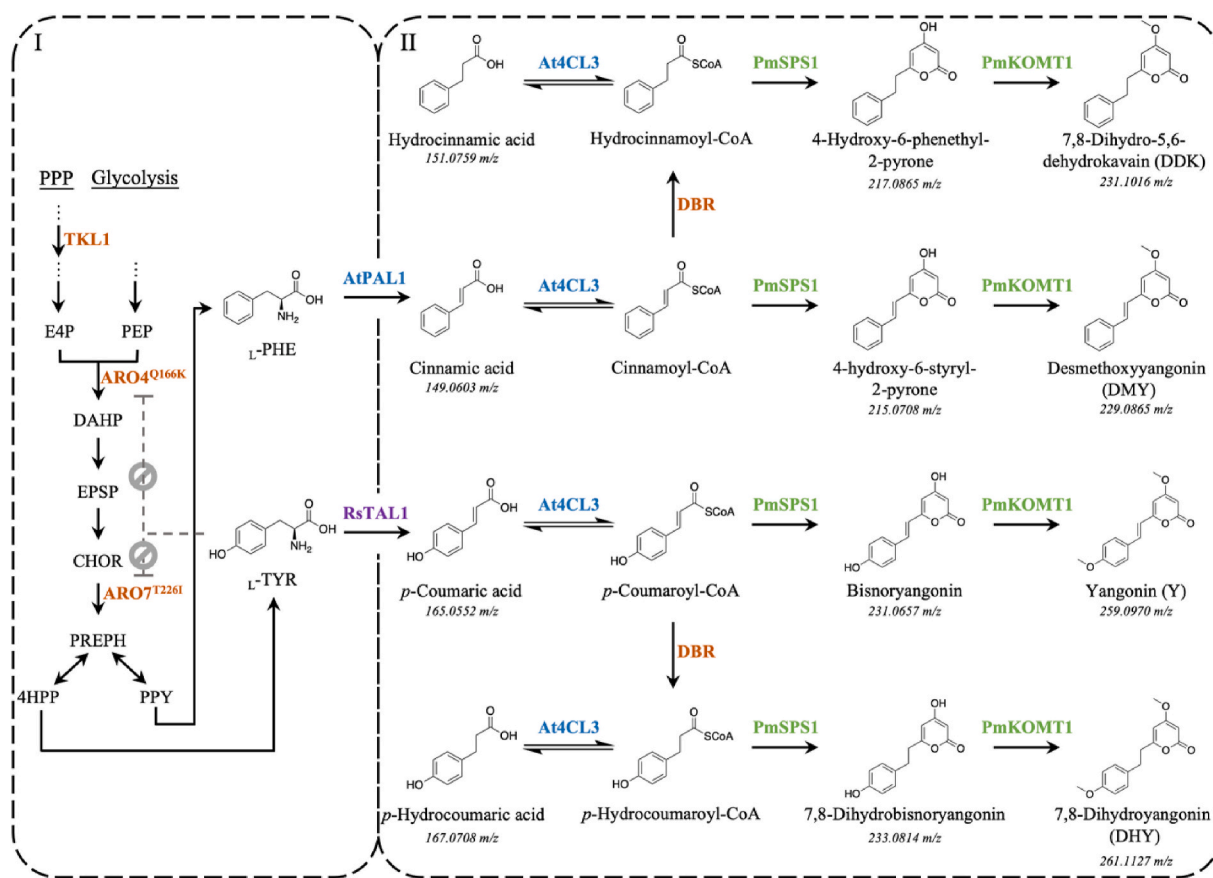
Fig. 1. Design of biosynthetic pathways for *de novo* production of four plant-derived styrylprones in *Saccharomyces cerevisiae*. Module I, parts of endogenous metabolic pathways and heterogeneous phenylpropanoid metabolism for overproduction of cinnamic acid and p-coumaric acid in *S. cerevisiae*; module II, 4-coumarate-CoA ligase, native double-bond redutases and core styrylprone biosynthetic pathways for production of plant styrylprones from cinnamic acid or p-coumaric acid. Enzymes marked in orange, blue, purple and green are from *S. cerevisiae*, *Arabidopsis*, *R. sphaeroides* and kava, respectively. Enzyme abbreviations: ARO3, phenylalanine-inhibited phospho-2-dehydro-3-deoxyheptonate aldolase; ARO4^{Q166K}, mutated phospho-2-dehydro-3-deoxyheptonate aldolase with relieved tyrosine-inhibition; ARO7^{T226I}, mutated chorismate mutase with relieved tyrosine-inhibition; At4CL3, 4-coumarate-CoA ligase 3; AtPAL1, phenylalanine ammonia-lyase 1; PmKOMT1, kava O-methyltransferases 1; PmSPS1, kava styrylpyrone synthase 1; RsTAL1, tyrosine ammonia-lyase; TKL1, transketolase 1. Metabolite abbreviations: 4HPP, 4-hydroxyphenylpyruvate; CHOR, chorismate; DAHP, 3-deoxy-D-arabinoheptulosonate-7-phosphate; E4P, D-erythrose-4-phosphate; EPSP, 5-enolpyruvyl-shikimate-3-phosphate; PEP, phosphoenolpyruvate; PHE, phenylalanine; PPY, phenylpyruvate; PREPH, prephenate; TYR, tyrosine. The number below compound name is corresponding m/z value of $[M+H]^+$. Co-substrates, co-factors and by-products are not shown. (For interpretation of the references to colour in this figure legend, the reader is referred to the Web version of this article.)

picked from the plates and used for *de novo* fermentation in YPD media in duplicates, followed by metabolite analysis.

3. Results

3.1. Design of complete biosynthetic pathways to enable diverse plant styrylpyrones production in yeast

The chemical diversity of plant styrylpyrones derives from different hydroxycinnamic acids (e.g., cinnamic, *p*-coumaric, and ferulic acids) as precursors, and/or the combination of downstream tailoring enzymes that further modify the styrylpyrone scaffold to diverse structures. Due to the lack of available plant gene resources (only the kava plant has been transcriptionally sequenced among all known styrylpyrone-producing plants), we addressed the product diversity issue by developing multiple upstream pathways producing diverse hydroxycinnamic acid precursors in yeast (Module I) and developing a core styrylpyrone biosynthetic pathway (Module II) that is able to convert these precursors to diverse plant-specific styrylpyrones (Fig. 1).

Leveraging the newly discovered kava SPS and OMT enzymes that have shown substrate promiscuity (Pluskal et al., 2019), we designed a core styrylpyrone biosynthetic pathway that is able to catalyze different hydroxycinnamoyl-CoAs (cinnamoyl-, *p*-coumaroyl-, hydrocinnamoyl-, and *p*-hydrocoumaroyl-CoAs) to corresponding styrylpyrones (DMY, Y, DDK, and DHY), respectively. Between the two kava SPSs identified (PmSPS1 and PmSPS2), PmSPS1 has proven functional in catalyzing multiple hydroxycinnamoyl-CoAs in *N. benthamiana* (Pluskal et al., 2019) and was thus selected for the core pathway construction. PmKOMT1 can methylate multiple hydroxyl groups at different positions of the styrylpyrone backbone and was selected to build the core pathway to enable the methylation at both the C4 and C12 positions. We completed the core pathway design by including *Arabidopsis thaliana* 4-coumarate-CoA ligase 3 (At4CL3), which is able to convert diverse hydroxycinnamic acids (cinnamic, *p*-coumaric, and ferulic acids) into corresponding CoA esters efficiently (Costa et al., 2005; Koopman et al., 2012). The resultant core styrylpyrone biosynthetic pathway (Module II) both enables the production of DDK, DHY, DMY, and Y and also has the potential to produce other plant styrylpyrones (for example, M and DHM that starts from feruloyl-CoA) in future engineering efforts.

We also designed *de novo* hydroxycinnamic acids biosynthetic pathways through a combination of genes derived from different organisms (Module I). Module I optimizes the yeast endogenous aromatic acid biosynthetic pathways to overproduce L-phenylalanine and L-tyrosine by exploiting yeast endogenous transketolase 1 (TKL1) in the pentose phosphate pathway and two tyrosine-inhibition insensitive enzyme mutants in the chorismite pathway, ARO4^{Q166K} (phospho-2-dehydro-3-deoxyheptonate aldolase variant) and ARO7^{T226I} (chorismate mutase variant) (Gold et al., 2015; Koopman et al., 2012; Li et al., 2015; Luttik et al., 2008; Trenchard et al., 2015); it also contains heterologous aromatic amino acid ammonia-lyase (*A. thaliana* phenylalanine ammonia-lyase (AtPAL1) (Cochrane et al., 2004) and *Rhodobacter sphaeroides* tyrosine ammonia-lyase (RsTAL1) (Jendresen et al., 2015)) to produce cinnamic acid and *p*-coumaric acid as styrylpyrone precursors. Although the kava or *A. zerumbet* genes leading to hydrocinnamic and *p*-hydrocoumaric acids syntheses remain unknown, our and other previous studies (Kong et al., 2020; Lehka et al., 2017) have proven that yeast endogenous double bond reductases (DBRs) are able to convert cinnamoyl-CoA and *p*-coumaroyl-CoA into hydrocinnamoyl-CoA and *p*-hydrocoumaroyl-CoA efficiently. Therefore, the yeast endogenous metabolism can be used to replace the unknown enzymes in plant and lead to the production of 7,8-saturated styrylpyrones such as DDK and DHY. Depending on whether the 7,8-bond is to be saturated, a yeast endogenous DBR, TSC13, is incorporated or deleted in Module I to direct the metabolic flux to either the DMY and Y pathways (unsaturated double bond) or the DDK and DHY pathways (saturated). As TSC13 is essential to yeast growth, a plant derived DBR

that does not catalyze hydroxycinnamoyl moieties, a *Malus domestica* enoyl reductase gene (*MdECR*), was chosen to replace endogenous *TSC13*, yielding a Δ*TSC13::MdECR* strain (ySL80), for DMY and Y production.

3.2. Reconstruction and characterization of a core biosynthetic pathway converting hydroxycinnamic acids to plant styrylpyrones (Module II)

To construct the core styrylpyrone pathway that converts hydroxycinnamic acids to the end-products, we codon-optimized the sequences of At4CL3, kava-derived PmSPS1, and PmKOMT1 for yeast expression, inserted them downstream of strong constitutive promoters (P_{TPI1}, P_{TEF1} and P_{PGK1}) in pSL85, pSL56, and pLS54 plasmids. The expression cassettes were integrated into the wild type CEN.PK2-1D, yielding ySL81, to leverage the native DBRs for the synthesis of DDK or DHY, respectively; the same cassettes were also integrated into the Δ*TSC13::MdECR* strain (ySL80) to yield ySL82 for the synthesis of DMY or Y, from cinnamic acid or *p*-coumaric acid, respectively (Fig. 2A). No growth inhibition was observed in ySL80 or ySL82 in all following tests, indicating that MdECR is able to complement the DBR activity of TSC13 for yeast growth.

We then validated and characterized the established pathway by feeding 200 μM cinnamic acid in cultured yeasts for 48 h (Fig. 2B and C). ySL82 that does not have the endogenous TSC13 was designed to produce pure DMY, while ySL81 was designed to produce DDK as the major product along with lower amount of DMY. As expected, the designated DMY producer, ySL82, produced 0.024 μM DMY from cinnamic acid (Fig. 2B). The low consumption of cinnamic acid (9.74 μM, 4.87% of total substrate) and no accumulation of hydrocinnamic acid in ySL82 proved that TSC13 is the major DBR catalyzing cinnamoyl-CoA in yeast (Fig. 2B and C). ySL81 produced 0.36 μM DDK in the fermentation (Fig. 2B). Although there was also 0.016 μM DMY accumulated as a downstream product of cinnamic acid instead of hydrocinnamic acid (Fig. 2B), the titer of DMY was only 4.44% of that of DDK in ySL81. The preferential production of DDK over DMY indicates the substrate preferences of PmSPS1 and/or PmKOMT1 for the hydrocinnamoyl moiety over the cinnamoyl moiety, which was firstly discovered in our study. It is worthy to note that the metabolic flux from hydrocinnamoyl moiety to DDK was not sufficient: despite of the complete consumption of cinnamic acid (Fig. 2C), the major product accumulated was hydrocinnamic acid (195.02 μM) (Fig. 2B), a putative product of the reversible reaction catalyzed by At4CL3 that converts excessive hydrocinnamoyl-CoA to hydrocinnamic acid.

We also fed 200 μM *p*-coumaric acid for DHY and Y production (Fig. 2D and E). ySL82 was designed to produce pure Y, while ySL81 was designed to produce DHY as the major product along with lower amount of Y. There was 0.021 μM Y produced in ySL82, which was 22.3-fold higher than the 0.0009 μM Y accumulation in ySL81 (Fig. 2D); the 22.3-fold enhancement is likely due to *TSC13* deletion that lowers the substrate competition between *p*-coumaroyl-CoA and *p*-hydrocoumaroyl-CoA. However, we were only able to observe two putative DHY precursors, 7,8-dihydrobisnoryangonin and 11-methoxy-7,8-dihydrobisnoryangonin, from ySL81 products via MS (233.0808 *m/z* (Figs. 2D) and 247.0965 *m/z* (Fig. S4)) and MS^2 (Fig. S5A, Fig. S5B) analyses, while DHY (261.1127 *m/z*) remained undetected. As there was abundant DHY substrate during fermentation (179.81 μM *p*-hydrocoumaric acid was accumulated, Fig. 2D), the less-efficient DHY biosynthetic pathway might be due to the substrate preference of the core pathway containing PmSPS1 and PmKOMT1.

3.3. Rate-limiting steps identification and optimization

ySL82 was able to produce pure, high-value DMY or Y in previous substrate feeding assays, thus is uniquely potential for future larger-scale biomanufacturing. However, only 2.5% cinnamic acid or 10% *p*-coumaric acid was consumed and an even smaller portion was converted to DMY and Y, which is likely due to the rate-limiting steps hindering
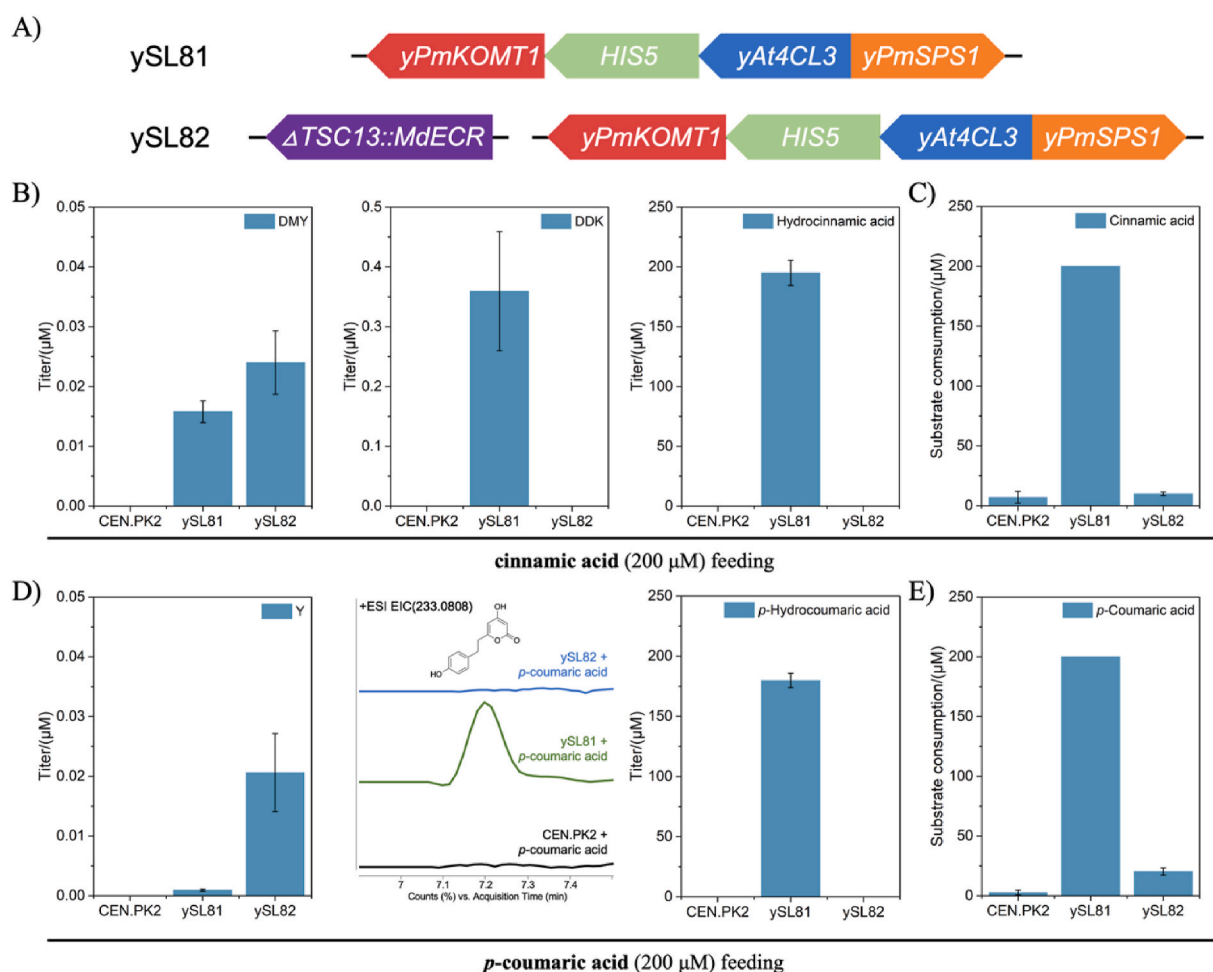
Fig. 2. Production of multiple plant-derived styrylpyrones through heterologous biosynthetic pathways after cinnamic acid or *p*-coumaric acid feeding. A) Genetic map of ySL81 and ySL82 strain. B) Product titers in cinnamic acid feeding assays. C) Substrate consumption in cinnamic acid feeding assays. D) Product titers in *p*-coumaric acid feeding assays. MS chromatography indicates the production of 7,8-dihydrobisnoryangonin ([M+H]$^+$ 233.0808, 20 ppm), a precursor of DHY. E) Substrate consumption in *p*-coumaric acid feeding assays. Substrate consumption and product titer was detected 48 h after substrates feeding. Gene abbreviations: *HIS5*, selection marker gene; *yAt4CL3*, codon-optimized *Arabidopsis* 4-coumarate-CoA ligase 3 gene; *yPmKOMT1*, codon-optimized kava O-methyltransferases 1 gene; yPmSPS1, codon-optimized kava styrylpyrone synthase 1 gene. Metabolite abbreviations: DMY, desmethoxyyangonin; DDK, 7,8-dihydro-5,6-dehydrokavain; Y, yangonin. Independent experiments, n = 3. Error bars represent standard deviation.

efficient metabolic flux towards the desired products. Thus, we started with ySL82 to identify and address the putative rate-limiting reactions via enzyme overexpression and combination. We overexpressed *yPmSPS1* and *yPmKOMT1* using high-copy plasmids (pRS424 and pRS426) respectively, resulting in pSL243 and pSL244 plasmids in ySL82 (Fig. 3). Overexpression of *yPmSPS1* increased the DMY titer from cinnamic acid by 10.5-fold from 0.024 μM to 0.28 μM; although overexpression of *yPmKOMT1* did not increase DMY production, the co-overexpression of both *yPmSPS1* and *yPmKOMT1* led to 15.7-fold increase to 0.40 μM DMY accumulation (Fig. 3A). The different performances after overexpression indicate that *yPmSPS1* was the initial rate-limiting step; the overexpression of *yPmSPS1* overcame such bottleneck and made its downstream reaction the new rate-limiting step, which was then overcome by the co-overexpression of *yPmKOMT1*. Meanwhile, overexpression also led to the production of trace amounts of DDK (0.043 μM when yPmSPS1 was overexpressed; 0.087 μM when yPmSPS1 and yPmKOMT1 were co-overexpressed (data not shown)), which was not observed before the optimization, and might result from other underlying yeast native DBRs. The ratios of DMY/DDK titer were 45 or higher, keeping DMY as the major final product as expected. Overexpression of *yPmSPS1* also increased Y accumulation from *p*-coumaric acid by 1.2-fold from 0.021 μM to 0.046 μM; overexpression of *yPmKOMT1* increased Y accumulation by 8.4-fold from 0.021 μM to 0.197

μM; and co-overexpression of *yPmSPS1* and *yPmKOMT1* led to 31-fold enhancement to 0.672 μM Y accumulation (Fig. 3B). We kept observing large variations when *yPmSPS1* and *yPmKOMT1* were co-overexpressed due to unknown reasons, which are possibly related with the pathway's cross talk with yeast's endogenous metabolism. No DHY was observed in all conditions. Overexpression of *yAt4CL3* in combination with other genes did not further improve DMY or Y production (data not shown). Therefore, co-expression of *yPmSPS1* and *yPmKOMT1* has a significant impact on increasing DMY and Y production. In addition, the overexpression of *yPmKOMT1* showed a higher production enhancement of Y than that of DMY; the varied demand of *yPmKOMT1* might result from the structural differences between Y and DMY, as the biosynthesis of Y involves the methylation of two hydroxyl groups at the C4 and C12 positions, and that of DMY only involves the O-methylation at the C4 position.
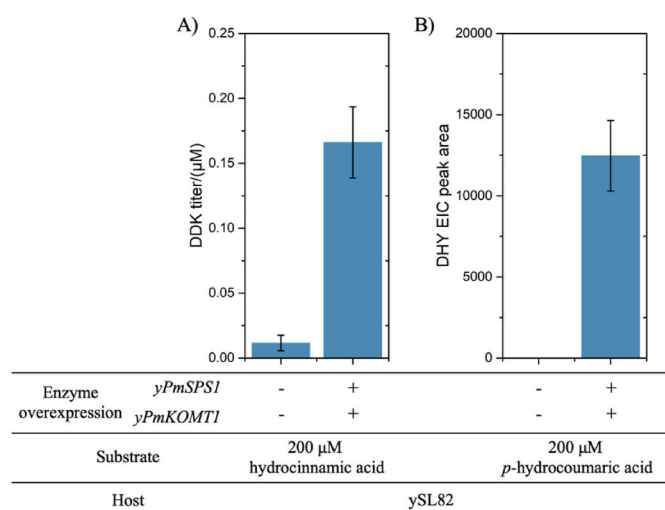
3.4. Production of DDK and DHY by feeding hydrocinnamic acids into engineered ySL82 strains

We then also explored the possibility of producing pure DDK or DHY by feeding 200 μM hydrocinnamic acid or *p*-hydrocoumaric acid into ySL82 (with or without co-overexpression of two rate-limiting enzymes) directly. In hydrocinnamic acid feeding assays, DDK production was
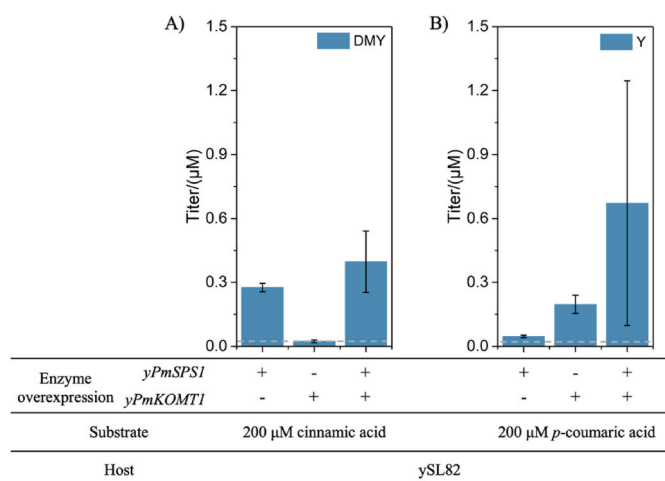
Fig. 3. Plasmid-based enzyme overexpression to identify rate-limiting enzymes and enhance the production of desmethoxyyangonin (DMY) and yangonin (Y) in substrate feeding assays. A) DMY titers of ySL82-derived strains, detected 48 h after cinnamic acid feeding. B) Y titers of ySL82-derived strains, detected 48 h after *p*-coumaric acid feeding. *yPmSPS1* and *yPmKOMT1* were overexpressed by introducing pSL243 and pSL244 plasmids into ySL82 hosts. - or +, with or without the corresponding plasmids. Gray dashed line, average titer of ySL82 strain after feeding 200 μM of corresponding substrate for 48 h. Gene abbreviations: *yPmKOMT1*, codon-optimized kava *O*-methyltransferases 1 gene; yPmSPS1, codon-optimized kava styrylpyrone synthase 1 gene. Error bars represent standard deviation, n=3 biological replicates.

enhanced by 13.8-fold from 0.012 to 0.166 μM after overexpressing (Fig. 4A). Surprisingly, the enhanced DDK titer is lower than that of ySL81 fed with cinnamic acid, indicating that the endogenous TSC13-mediated hydrocinnamoyl-CoA production mechanism is preferred due to unknown synergistic effect. In *p*-hydrocoumaric acid feeding assays, a putative peak (261.1127 *m/z*) of DHY (structurally characterized via MS^2 analysis (Fig. S6)) was eventually observed (Fig. 4B), showing the pathway capacity of DHY production. Although we did not

further optimize the production due to the lack of DHY standard and appropriate analytical methods, feeding *p*-hydrocoumaric acid into an optimized yeast strain is a promising method for DHY production.

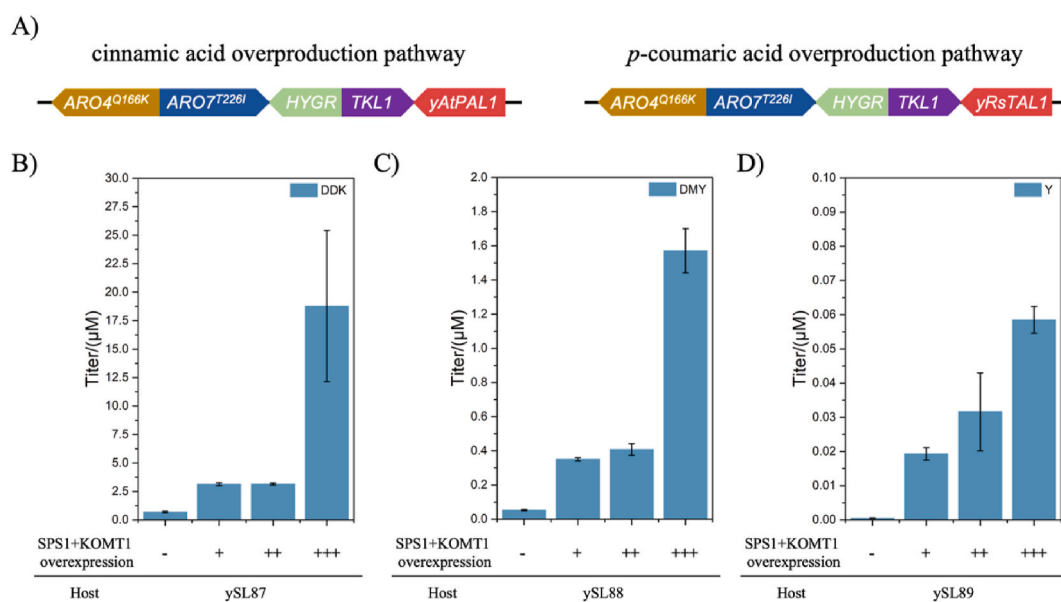### 3.5. Module I pathway reconstruction and de novo production of DDK, DMY and Y

Aiming for the complete biosynthesis of the high-value DDK, DMY and Y in yeast, we firstly integrated two diverse upstream Module I pathways (Figs. 1A and 5A) into the genome of the ySL80 (ΔTSC13::*MdECR*), resulting in ySL84 for cinnamic acid production and ySL86 for *p*-coumaric acid production; the pathways were also integrated into the genome of CEN.PK2-1D, resulting in ySL83 and ySL85 respectively, to leverage the endogenous DBR activity for hydrocinnamoyl-CoA and *p*-hydrocoumaroyl-CoA production when At4CL3 in the Module II is also present during complete biosynthesis. After 48 h of fermentation in SC media, ySL84 and ySL86, produced 62 μM cinnamic acid and 11 μM of *p*-coumaric acid (Fig. S7), respectively. The strains with endogenous TSC13, ySL83 and ySL85, produced 330 μM cinnamic acid and 47 μM *p*-coumaric acid (Fig. S7), respectively. The lower production of both cinnamic acid and *p*-coumaric acid in ΔTSC13::*MdECR* strains (ySL84 and ySL86) might be due to an unknown inhibitory effect derived from hydroxycinnamic acids on yeast endogenous metabolism that was alleviated in the presence of TSC13.

We then combined Module I with the Module II pathway to construct the complete biosynthetic strains. The cinnamic acid biosynthetic pathway module was integrated into ySL81 for DDK complete biosynthesis (ySL87); the cinnamic acid biosynthetic pathway module was also integrated into ySL82 (ΔTSC13::*MdECR*) strain that mainly produces cinnamoyl-CoA for DMY complete biosynthesis (ySL88); the *p*-coumaric acid biosynthetic pathway module was integrated into the ySL82 (ΔTSC13::*MdECR*) strain for Y production (ySL89). The three complete biosynthetic pathways led to 0.69, 0.053 and 0.0056 μM DDK, DMY, and Y production as the major products, respectively (Fig. 5B, C and D) after 48 h cultivation in SD media. Both DDK and DMY titers are higher than those in ySL81 and ySL82 (0.36 and 0.024 μM) which contain Module II only and are fed with 200 μM cinnamic acid; while the titer of Y via complete synthesis (0.0056 μM) is lower than that in ySL82 (0.021 μM) fed with 200 μM *p*-coumaric acid. The accumulations of corresponding hydroxycinnamic acid precursors also vary; there were significant accumulations of the DDK and DMY upstream precursors (175 μM hydrocinnamic acid and 35 μM cinnamic acid) in comparison with the upstream precursor of Y (2.5 μM coumaric acid). Therefore, the enhanced titers in the DDK and DMY complete biosynthetic strains, along with the lower production of Y, are possibly associated with the strains' varied production efficiency of upstream hydroxycinnamic acid precursors (Module I), the substrate preferences of the core pathway (Module II), and yeast's tolerances on inhibitory hydroxycinnamic acids.

3.6. Production enhancement by multi-copy Module II pathway overexpression via CRISPR-based δ-integration

We further overexpressed the identified rate-limiting enzymes in ySL87, ySL88, and ySL89 for enhanced DDK, DMY, and Y production. The accumulation of hydroxycinnamic acids in ySL87-89 indicates that the biosynthetic efficiency of Module II cannot match that of Module I. Therefore, we tuned the overexpression level of PmSPS1 and PmKOMT1 by overexpressing *yPmSPS1-yPmKOMT1* in the widely-used high-copy plasmid pRS425 and two optimized plasmids with higher copy numbers (named ultra-high-copy plasmids): to achieve a higher copy number, the promoters driving the expression of the *LEU2* or *URA3* marker in pRS425 or pRS426 plasmid were truncated to yield higher plasmid copies in corresponding synthetic dropout media, resulting in the pRS425-LEU2d (pSL202) and pRS426-URA3d (pSL203) plasmids. *mCherry* intensity assay using these plasmids (Fig. S8) showed that, compared with pRS425, pSL202 and pSL203 led to 2- and 4.8-fold

Fig. 4. Hydrocinnamic acid and *p*-hydrocoumaric acid feeding assays of ySL82 derived strains. A) DDK titers of ySL82-derived strains, detected 48 h after hydrocinnamic acid feeding. B) DHY production of ySL82-derived strains, detected 48 h after *p*-hydrocoumaric acid feeding. *yPmSPS1* and *yPmKOMT1* were overexpressed by introducing pSL243 and pSL244 plasmids into ySL82 hosts. - or +, with or without the corresponding plasmids. Gene abbreviations: *yPmKOMT1*, codon-optimized kava *O*-methyltransferases 1 gene; *yPmSPS1*, codon-optimized kava styrylpyrone synthase 1 gene. Error bars represent standard deviation, n=3 biological replicates.

Fig. 5. *De novo* overproduction of 7,8-dihydro-5,6-dehydrokavain (DDK), desmethoxyyangonin (DMY) and yangonin (Y). A) Genetic map of cinnamic acid and *p*-coumaric acid overproduction pathway. Cinnamic acid biosynthetic pathway was integrated into strain ySL81 and ySL82 genome to construct strain ySL87 and ySL88 for DDK and DMY *de novo* production, respectively. *p*-Coumaric acid biosynthetic pathway was integrated into strain ySL82 genome to generate strain ySL89 for Y *de novo* production. B), C) and D), DDK, DMY and Y titers of the corresponding strains, detected after 48 h of fermentation. Rate-limiting enzymes were overexpressed on plasmids to enhance the production. -, host without plasmids; +, host with pSL252 plasmids (with high copy number); ++, host with pSL253 plasmids (with higher copy number); +++, host with pSL254 (with ultra-high copy number). Gene abbreviations: $ARO4^{Q166K}$, feedback inhibition-relieved *S. cerevisiae* tyrosine-inhibited phospho-2-dehydro-3-deoxyheptonate aldolase gene; $ARO7^{T226I}$, feedback inhibition-relieved *S. cerevisiae* chorismate mutase gene; *TKL1*, transketolase 1 gene; *yAtPAL1*, codon-optimized *Arabidopsis* phenylalanine ammonia-lyase 1 gene; *yRsTAL1*, codon-optimized *R. sphaeroides* tyrosine ammonia-lyase gene. Error bars represent standard deviation, n=3 biological replicates.

expression increase, respectively. pRS425, pSL202, and pSL203 that harbor both y*PmSPS1 and yPmKOMT1* (pSL252, pSL253, and pSL254, respectively) were transformed into ySL87, ySL88, and ySL89 and compared. pSL203 that is associated with the highest copy number exhibited the highest DDK, DMY and Y production, each increased by up to 27.1-, 29.6- and 10.5-fold, to 18.7, 1.57 and 0.059 μM, respectively (Fig. 5).

Aiming at developing robust and stable styrylpyrone-producing yeasts that are compatible with industrial fermentation, we then used and customized the CRISPR-based δ-integration (Shi et al., 2016) method to achieve multicopy genomic integration. Additional fragments expressing *yPmSPS*1 and *yPmKOMT1* were integrated into the yeast δ-transposon sites with flanking regions homologous to the δ-site sequences ($δ_L$ and $δ_R$), facilitated by a plasmid harboring *Cas9* and δ site-targeting gRNA (pSL257) (Fig. 6A). To increase the integration efficiency, a heterogeneous *KlLEU2d* selection marker was fused with the inserts; resultant fragment ($δ_L$-*KlLEU2d*-y*PmSPS1*-y*PmKOMT1*-$δ_R$) was cotransformed with pSL257 into ySL87, ySL88 and ySL89, respectively. After removing pSL257, successful integrants were prescreened for styrylpyrone production in synthetic dropout media (Fig. S9, Fig. S10 and Fig. S11) and showed higher production than the original ones. The strains were named as ySL87-δ_SK, ySL88-δ_SK and ySL89-δ_SK and validated with replicates to confirm the enhanced production (Fig. 6B, C and D). Compared with corresponding parental strains, the titer of DDK, DMY, and Y of ySL87-δ_SK, ySL88-δ_SK, and ySL89-δ_SK in synthetic dropout medium increased by 1.2-, 17.3-, and 10-fold, to 1.54, 0.97 and 0.06 μM respectively. The stable δ-integration further enhanced production in rich YPD media to 4.40 μM DDK, 1.29 μM DMY, and 0.10 μM Y. Finally, we confirmed that the high-titer phenotype of overproducers was stably maintained after around 50 generations of growth in YPD media (Fig. S12), allowing for further engineering and industrial application.

4. Discussion and conclusions

We leveraged a recently discovered kava styrylpyrone biosynthetic pathway and a combination of diverse genes that produce different hydroxycinnamic acids to enable the complete biosynthesis of diverse, plant-specific, and high-value styrylpyrones. The yeast strains developed firstly enabled the complete and optimized biosynthesis of high-value DDK, DMY and Y and demonstrated the potential of DHY biosynthesis that can be further optimized in future work. Taking advantages of the substrate promiscuity of core enzymes, two different aromatic acid ammonia-lyases and one native double-bond reductase were combinatorially applied with six other enzymes to direct the metabolite flux into different final products. The resultant ySL87, ySL88 and ySL89 produced DDK, DMY, DHY from simple carbon and nitrogen sources at titers of 0.69, 0.053 and 0.0056 μM, respectively. Overexpression of rate-limiting enzymes (PmSPS1 and PmKOMT1) through CRISPR-based δ-integration resulted in three robust overproducers, whose titers dramatical increased to 4.40, 1.29 and 0.10 μM in YPD media, respectively. Although the titers are still low for commercial biomanufacturing, this work highlights the feasibility of yeast for psychoactive or nutritional plant styrylpyrones biosynthesis; it also demonstrates that the combination of heterologous genes and the yeast endogenous metabolism can enable the biosynthesis of rare PNPs, even ones for which the native plant biosynthetic pathways have not been fully elucidated.

Our heterologous fermentation results indicate that the low efficiencies of PmSPS1 and PmKOMT1 are the major bottleneck hindering efficient styrylpyrone production. Discovery and functional expression of enzymes from other plants might solve this problem: *Equisetum arvense* styrylpyrone synthase 3 (Beckert et al., 1997), *Humulus lupulus* chalcone synthase (Okada et al., 2004) *Neonothopanus nambi* hispidin synthase (Kotlobay et al., 2018), and *Piper nigrum* polyketide synthase (Heo et al., 2021) that have been reported to catalyze the formation of styrylpyrone scaffolds are potential candidates for future investigations;
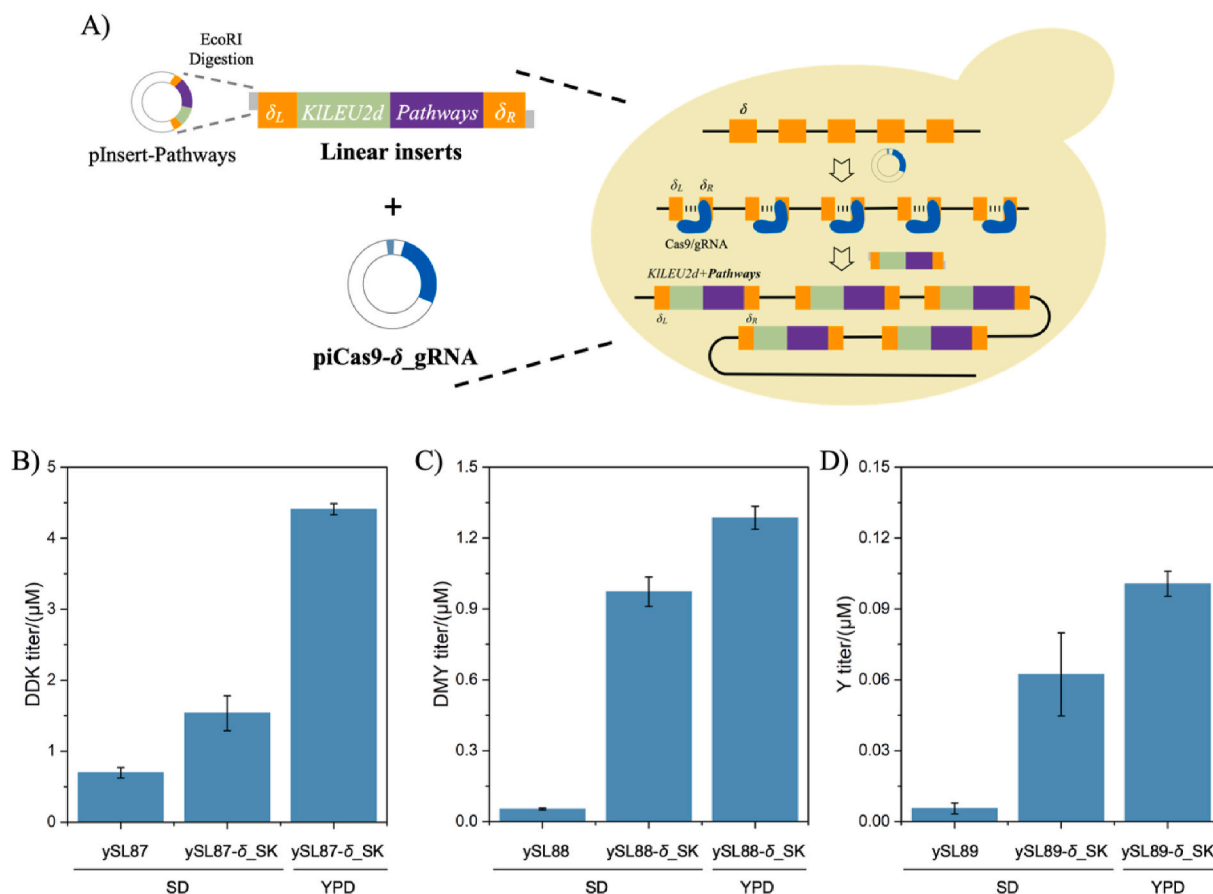
Fig. 6. CRISPR/Cas9-mediated δ-integration of rate-limiting enzyme overexpression casettes to enhance plant-derived styrylprone *de novo* production. A) CRISPR/Cas9-mediated δ-integration schematic. First, pathways without EcoRI cutting sites are inserted between *KlLEU2d* and δ_R to constitute pInsert-Pathways plasmids via Gibson assembly. After EcoRI digestion, the purified linear inserts with δ_L and δ_R homologous arms are cotransformed into *S. cerevisiae* with piCas9-δ_gRNA (pSL257) plasmids to induce the integration of pathways at multiple δ sites. *KlLEU2d* marker is applied for selection of true positives herein. Finally, piCas9-δ_gRNA plasmids are removed by 5-fluoroorotic acid (5-FOA) counter-selection to get the robust overproducers. B), C) and D), the titer of original host and selected overproducers after δ-integration in SD or YPD media. Metabolite abbreviations: DMY, desmethoxyyangonin; DDK, 7,8-dihydro-5,6-dehydrokavain; Y, yangonin. Error bars represent standard deviation, n=3 biological replicates.

A. zerumbet that exhibits high DDK productivity might provide novel styrylpyrone synthases and *O*-methyltransferases. In addition, the development of computational protein design has opened up the opportunity of designing novel enzymes from a known template (Planas-Iglesias et al., 2021). We anticipate engineered PmSPS1 and PmKOMT1 variants will further enhance heterologous production. Meanwhile, there is an obvious trade-off between the cell growth rate and the production of styrylpyrones, indicating the further endogenous metabolism rewiring would promote efficient styrylpyrone production. Although the production of plant styrylpyrone in yeast had not been reported before, great efforts have been made in the production of naringenin or other flavonoids through plant type III polyketide synthase (Milke and Marienhagen, 2020) that share similar upstream enzymes and cofactors. Accordingly, by rewiring carbon metabolism for high level production of aromatic precursors, regulating malonyl-CoA flux, enhancing *S*-adenosyl methionine availability, and optimizing media and fermentation, we anticipate plant styrylpyrone titers being further increased.

Plants with medicinal or health-promoting potentials are usually used as complex mixtures. It is essential yet difficult to isolate the individual components from the large number of PNPs that have high structural similarity. Thus, the ability to synthesize structurally similar PNPs individually using functionally specific yeast strains is important to fully understand the biological activity of medicinal plants and to discover effective PNPs as novel drug candidates. There are two ways to

regenerate the diversity of PNPs in nature: using one or more differential tailoring enzymes to modify a specific chemical scaffold or using structurally similar but distinct substrates that will lead to diverse chemical scaffolds (Anarat-Cappillino and Sattely, 2014). The former remains challenging for yeast-based biosynthesis, as the vast majority of plant styrylpyrone biosynthetic pathways and enzymes remain unknown and the kava-derived oxidoreductases (PmKLR1 and PmCYP719A26) have not been functionally expressed in yeast in previous publication (Pluskal et al., 2019) or our study (data not shown). Meanwhile, the latter provides a promising, combinatorial biosynthesis approach that can be translated into an artificial, yeast-based biosynthetic system. Therefore, we designed a promiscuous core styrylpyrone biosynthetic pathway that can incorporate diverse hydroxycinnamic acids to generate different styrylpyrone scaffolds and enable the plant-specific C4 position *O*-methylation. To provide diverse substrates (hydrocinnamoyl-acids) to the core pathway, we reconstituted the hydroxycinnamic acid biosynthetic pathways in yeast: cinnamic acid and *p*-coumaric acid are two important and well-studied hydroxycinnamic acids in plant phenylpropanoid metabolism, and we managed to reconstruct two pathways and corresponding yeast strains (ySL84 and ySL86) that are designated to produce one compound each. Hydrocinnamic acid and *p*-hydrocoumaric acid have also been proven important in plant specialized metabolism, yet the associated biosynthetic pathways have not been well understood. We leveraged the yeast endogenous metabolism (mainly TSC13) that efficiently reduces

cinnamoyl- and *p*-coumaroyl-CoAs to complement the missing step, thus avoiding the search for plant DBRs and enabling hydrocinnamoyl- and *p*-hydrocoumaroyl-CoA production. In addition, it is likely that the plant-derived 4-coumarate-CoA ligase (At4CL3) exhibits unexpected high catalytic activity that converts excessive hydrocinnamoyl- and *p*-hydrocoumaroyl-CoA to corresponding acids; although the 4CL-catalyzed reaction is known to be reversible, At4CL3 in yeast favors the reversed hydrolysis reaction as opposed to the ligation reaction as in plants, ultimately leading to the development of two novel yeast strains that mainly provide hydrocinnamoyl- and *p*-hydrocoumaroyl moieties for downstream PNP synthesis. Pairing the four upstream precursor biosynthetic pathways with the promiscuous core styrylpyrone pathway led to four individual yeast strains that produce DDK, DMY, Y, and DHY with little to no byproducts. The biosynthetic potential of these pathway modules can be further expanded, as we have also observed trace amounts of pathway intermediates that are potential M or DHM precursors (Fig. S13) in ySL82 fed with ferulic acid or hydroferulic acid. In summary, combinatorial biosynthesis has proven an effective approach for producing natural or novel synthetic compounds, particularly fungal-derived natural products (Kim et al., 2015), but its applications for PNP synthesis were mainly demonstrated in *N. benthamiana* (Eljounaidi and Lichman, 2020) or *E. coli* (Lin et al., 2013). Our work provides more evidence to prove the feasibility of this approach in yeast as an industrial microorganism for large-scale and safe biomanufacturing of diverse valuable PNPs.

CRediT authorship contribution statement

Yinan Wu: Conceptualization, Methodology, Investigation, Validation, Data curation, Formal analysis, Visualization, Writing – original draft. **Maple N. Chen:** Resources, Investigation, Validation, Writing – review & editing. **Sijin Li:** Conceptualization, Supervision, Project administration, Funding acquisition, Writing – review & editing.

Declaration of competing interest

A provisional application for patent has been filed listing Y.W. and S. L. as inventors.

Appendix A. Supplementary data

Supplementary data to this article can be found online at https://doi. org/10.1016/j.mec.2022.e00195.

References

Ali Shaik, A., Tan, J., Lü, J., Xing, C., 2012. Economically viable efficient synthesis of (±)-methysticin: a component in kava potentially responsible for its cancer chemopreventive activity. Arkivoc 137–145. https://doi.org/10.3998/ark.5550190.0013.813, 2012.

Anarat-Cappillino, G., Sattely, E.S., 2014. The chemical logic of plant natural product biosynthesis. Curr. Opin. Plant Biol. 19, 51–58. https://doi.org/10.1016/j.pbi.2014.03.007.

Bao, Z., Xiao, H., Liang, J., Zhang, L., Xiong, X., Sun, N., Si, T., Zhao, H., 2015. Homology-integrated CRISPR-Cas (HI-CRISPR) system for one-step multigene disruption in *Saccharomyces cerevisiae*. ACS Synth. Biol. 4, 585–594. https://doi.org/10.1021/sb500255k.

Beckert, C., Horn, C., Schnitzler, J.P., Lehning, A., Heller, W., Veit, M., 1997. Styrylpyrone biosynthesis in *Equisetum arvense*. Phytochemistry 44, 275–283. https://doi.org/10.1016/S0031-9422(96)00543-2.

Bian, T., Corral, P., Wang, Y., Botello, J., Kingston, R., Daniels, T., Salloum, R.G., Johnston, E., Huo, Z., Lu, J., Liu, A.C., Xing, C., 2020. Kava as a clinical nutrient: promises and challenges. Nutrients 12, 3044. https://doi.org/10.3390/nu12103044.

Blount, Z.D., Borland, C.Z., Lenski, R.E., 2008. Historical contingency and the evolution of a key innovation in an experimental population of *Escherichia coli*. Proc. Natl. Acad. Sci. U.S.A. 105, 7899–7906. https://doi.org/10.1073/pnas.0803151105.

Cochrane, F.C., Davin, L.B., Lewis, N.G., 2004. The *Arabidopsis* phenylalanine ammonia lyase gene family: kinetic characterization of the four PAL isoforms. Phytochemistry 65, 1557–1564. https://doi.org/10.1016/j.phytochem.2004.05.006.

Costa, M.A., Bedgar, D.L., Moinuddin, S.G.A., Kim, K., Cardenas, C.L., Cochrane, F.C., Shockey, J.M., Helms, G.L., Amakura, Y., Takahashi, H., Milhollan, J.K., Davin, L.B., Browse, J., Lewis, N.G., 2005. Characterization *in vitro* and *in vivo* of the putative multigene 4-coumarate:CoA ligase network in *Arabidopsis*: syringyl lignin and sinapate/sinapyl alcohol derivative formation. Phytochemistry 66, 2072–2091. https://doi.org/10.1016/j.phytochem.2005.06.022.

Courdavault, V., O'Connor, S.E., Jensen, M.K., Papon, N., 2021. Metabolic engineering for plant natural products biosynthesis: new procedures, concrete achievements and remaining limits. Nat. Prod. Rep. 38, 2145. https://doi.org/10.1039/d0np00092b.

Eljounaidi, K., Lichman, B.R., 2020. Nature's Chemists: the discovery and engineering of phytochemical biosynthesis. Front. Chem. 8, 596479. https://doi.org/10.3389/fchem.2020.596479.

Gibson, D.G., Young, L., Chuang, R.-Y., Venter, J.C., Hutchison, C.A., Smith, H.O., 2009. Enzymatic assembly of DNA molecules up to several hundred kilobases. Nat. Methods 6, 343–345. https://doi.org/10.1038/nmeth.1318.

Gold, N.D., Gowen, C.M., Lussier, F.X., Cautha, S.C., Mahadevan, R., Martin, V.J.J., 2015. Metabolic engineering of a tyrosine-overproducing yeast platform using targeted metabolomics. Microb. Cell Factories 14, 73. https://doi.org/10.1186/s12934-015-0252-2.

Han, J., Wu, Y., Zhou, Y., Li, S., 2021. Engineering *Saccharomyces cerevisiae* to produce plant benzylisoquinoline alkaloids. aBIOTECH 432. https://doi.org/10.1007/s42994-021-00055-0.

Heo, K.T., Lee, B., Jang, J.-H., Ahn, J.-O., Hong, Y.-S., 2021. Construction of an artificial biosynthetic pathway for the styrylpyrone compound 11-methoxy-bisnoryangonin produced in engineered *Escherichia coli*. Front. Microbiol. 12, 714335. https://doi.org/10.3389/fmicb.2021.714335.

Israili, Z.H., Smissman, E.E., 1976. Synthesis of kavain, dihydrokavain, and analogues. J. Org. Chem. 41, 4070–4074. https://doi.org/10.1021/jo00888a004.

Jendresen, C.B., Stahlhut, S.G., Li, M., Gaspar, P., Siedler, S., Förster, J., Maury, J., Borodina, I., Nielsen, A.T., 2015. Highly active and specific tyrosine ammonia-lyases from diverse origins enable enhanced production of aromatic compounds in bacteria and *Saccharomyces cerevisiae*. Appl. Environ. Microbiol. 81, 4458–4476. https://doi.org/10.1128/AEM.00405-15.

Kim, E., Moore, B.S., Yoon, Y.J., 2015. Reinvigorating natural product combinatorial biosynthesis with synthetic biology. Nat. Chem. Biol. 11, 649–659. https://doi.org/10.1038/nchembio.1893.

Kong, D., Li, S., Smolke, C.D., 2020. Discovery of a previously unknown biosynthetic capacity of naringenin chalcone synthase by heterologous expression of a tomato gene cluster in yeast. Sci. Adv. 6, eabd1143. https://doi.org/10.1126/sciadv.abd1143.

Koopman, F., Beekwilder, J., Crimi, B., van Houwelingen, A., Hall, R.D., Bosch, D., van Maris, A.J. a, Pronk, J.T., Daran, J.-M., 2012. *De novo* production of the flavonoid naringenin in engineered *Saccharomyces cerevisiae*. Microb. Cell Factories 11, 155. https://doi.org/10.1186/1475-2859-11-155.

Kotlobay, A.A., Sarkisyan, K.S., Mokrushina, Y.A., Marcet-Houben, M., Serebrovskaya, E. O., Markina, N.M., Somermeyer, L.G., Gorokhovatsky, A.Y., Vvedensky, A., Purtov, K.V., Petushkov, V.N., Rodionova, N.S., Chepurnyh, T.V., Fakhranurova, L.I., Guglya, E.B., Ziganshin, R., Tsarkova, A.S., Kaskova, Z.M., Shender, V., Abakumov, M., Abakumova, T.O., Povolotskaya, I.S., Eroshkin, F.M., Zaraisky, A.G., Mishin, A.S., Dolgov, S.V., Mitiouchkina, T.Y., Kopantzev, E.P., Waldenmaier, H.E., Oliveira, A.G., Oba, Y., Barsova, E., Bogdanova, E.A., Gabaldón, T., Stevani, C.V., Lukyanov, S., Smirnov, I.V., Gitelson, J.I., Kondrashov, F.A., Yampolsky, I.V., 2018. Genetically encodable bioluminescent system from fungi. Proc. Natl. Acad. Sci. U.S. A. 115, 12728–12732. https://doi.org/10.1073/pnas.1803615115.

Kraus, G.A., Wanninayake, U.K., 2015. An improved aldol protocol for the preparation of 6-styrenylpyrones. Tetrahedron Lett. 56, 7112–7114. https://doi.org/10.1016/j.tetlet.2015.11.021.

Lee, I.K., Yun, B.S., 2011. Styrylpyrone-class compounds from medicinal fungi *Phellinus* and *Inonotus* spp., and their medicinal importance. J. Antibiot. (Tokyo) 64, 349–359. https://doi.org/10.1038/ja.2011.2.

Lehka, B.J., Eichenberger, M., Bjørn-Yoshimoto, W.E., Vanegas, K.G., Buijs, N., Jensen, N.B., Dyekjær, J.D., Jenssen, H., Simon, E., Naesby, M., 2017. Improving heterologous production of phenylpropanoids in *Saccharomyces cerevisiae* by tackling an unwanted side reaction of Tsc13, an endogenous double-bond reductase. FEMS Yeast Res. 17, fox004. https://doi.org/10.1093/femsyr/fox004.

Li, M., Kildegaard, K.R., Chen, Y., Rodriguez, A., Borodina, I., Nielsen, J., 2015. *De novo* production of resveratrol from glucose or ethanol by engineered *Saccharomyces cerevisiae*. Metab. Eng. 32, 1–11. https://doi.org/10.1016/j.ymben.2015.08.007.

Li, S., Li, Y., Smolke, C.D., 2018. Strategies for microbial synthesis of high-value phytochemicals. Nat. Chem. 10, 395–404. https://doi.org/10.1038/s41557-018-0013-z.

Li, Y., Li, S., Thodey, K., Trenchard, I., Cravens, A., Smolke, C.D., 2018. Complete biosynthesis of noscapine and halogenated alkaloids in yeast. Proc. Natl. Acad. Sci. U.S.A. 115, E3922–E3931. https://doi.org/10.1073/pnas.1721469115.

Lin, L., Chen, Z., Yang, X., Liu, X., Feng, X., 2008. Efficient enantioselective hetero-Diels-Alder reaction of Brassard's diene with aliphatic aldehydes: a one-step synthesis of (R)-(+)-kavain and (S)-(+)-dihydrokavain. Org. Lett. 10, 1311–1314. https://doi.org/10.1021/ol8002282.

Lin, Y., Sun, X., Yuan, Q., Yan, Y., 2013. Combinatorial biosynthesis of plant-specific coumarins in bacteria. Metab. Eng. 18, 69–77. https://doi.org/10.1016/j.ymben.2013.04.004.

Luttik, M.A.H., Vuralhan, Z., Suir, E., Braus, G.H., Pronk, J.T., Daran, J.M., 2008. Alleviation of feedback inhibition in *Saccharomyces cerevisiae* aromatic amino acid biosynthesis: quantification of metabolic impact. Metab. Eng. 10, 141–153. https://doi.org/10.1016/j.ymben.2008.02.002.

Milke, L., Marienhagen, J., 2020. Engineering intracellular malonyl-CoA availability in microbial hosts and its impact on polyketide and fatty acid synthesis. Appl. Microbiol. Biotechnol. 104, 6057–6065. https://doi.org/10.1007/s00253-020-10643-7.

Okada, Y., Sano, Y., Kaneko, T., Abe, I., Noguchi, H., Ito, K., 2004. Enzymatic reactions by five chalcone synthase homologs from hop (*Humulus lupulus* L.). Biosci. Biotechnol. Biochem. 68, 1142–1145. https://doi.org/10.1271/bbb.68.1142.

Planas-Iglesias, J., Marques, S.M., Pinto, G.P., Musil, M., Stourac, J., Damborsky, J., Bednar, D., 2021. Computational design of enzymes for biotechnological applications. Biotechnol. Adv. 47, 107696. https://doi.org/10.1016/j.biotechadv.2021.107696.

Pluskal, T., Torrens-spence, M.P., Fallon, T.R., Abreu, A. De, Shi, C.H., 2019. The biosynthetic origin of psychoactive kavalactones in kava. Native Plants 5, 867–878. https://doi.org/10.1038/s41477-019-0474-0.

Pyne, M.E., Narcross, L., Martin, V.J.J., 2019. Engineering plant secondary metabolism in microbial systems. Plant Physiol. 179, 844–861. https://doi.org/10.1104/pp.18.01291.

Sarris, J., Stough, C., Bousman, C.A., Wahid, Z.T., Murray, G., Teschke, R., Savage, K.M., Dowell, A., Ng, C., Schweitzer, I., 2013. Kava in the treatment of generalized anxiety disorder: a double-blind, randomized, placebo-controlled study. J. Clin. Psychopharmacol. 33, 643–648. https://doi.org/10.1097/JCP.0b013e318291be67.

Shi, S., Liang, Y., Zhang, M.M., Ang, E.L., Zhao, H., 2016. A highly efficient single-step, markerless strategy for multi-copy chromosomal integration of large biochemical pathways in *Saccharomyces cerevisiae*. Metab. Eng. 33, 19–27. https://doi.org/10.1016/j.ymben.2015.10.011.

Smith, K., Leiras, C., 2018. The effectiveness and safety of Kava Kava for treating anxiety symptoms: a systematic review and analysis of randomized clinical trials. Complement. Ther. Clin. Pract. 33, 107–117. https://doi.org/10.1016/j.ctcp.2018.09.003.

Song, M.C., Kim, E.J., Kim, E., Rathwell, K., Nam, S., Yoon, Y.J., 2014. Microbial biosynthesis of medicinally important plant secondary metabolites. Nat. Prod. Rep. 31, 1497. https://doi.org/10.1039/C4NP00057A.

Teschke, R., Xuan, T.D., 2018. Viewpoint: a contributory role of shell ginger (*Alpinia zerumbet* (Pers.) B.L. Burtt & R.M. Sm) for human longevity in Okinawa, Japan? Nutrients 10, 166. https://doi.org/10.3390/nu10020166.

Trenchard, I.J., Siddiqui, M.S., Thodey, K., Smolke, C.D., 2015. *De novo* production of the key branch point benzylisoquinoline alkaloid reticuline in yeast. Metab. Eng. 31, 74–83. https://doi.org/10.1016/j.ymben.2015.06.010.

Tu, P.T.B., Tawata, S., 2014. Anti-obesity effects of hispidin and *Alpinia zerumbet* bioactives in 3T3-L1 adipocytes. Molecules 19, 16656–16671. https://doi.org/10.3390/molecules191016656.

Tzeng, Y.M., Lee, M.J., 2015. Neuroprotective properties of kavalactones. Neural Regen. Res. 10, 875–877. https://doi.org/10.4103/1673-5374.158335.

Volgin, A., Yang, L.E., Amstislavskaya, T., Demin, K., Wang, D., Yan, D., Wang, J., Wang, M., Alpyshov, E., Hu, G., Serikuly, N., Shevyrin, V., Wappler-Guzzetta, E., De Abreu, M., Kalueff, A., 2020. Dark classics in chemical neuroscience: Kava. ACS Chem. Neurosci. 11, 3893–3904. https://doi.org/10.1021/acschemneuro.9b00587.

Xuan, T.D., Teschke, R., 2015. Dihydro-5,6-dehydrokavain (DDK) from *Alpinia zerumbet*: its isolation, synthesis, and characterization. Molecules 20, 16306–16319. https://doi.org/10.3390/molecules200916306.

Zhang, N., Wu, L., Liu, X., Shen, X., 2018. Plant-derived kavalactones and their bioactivities. Med. Res. Res. 2, 170019. https://doi.org/10.21127/yaoyimr20170019.